Trial shadow wave function for the ground state of ^{4}He

T. MacFarland
Laboratory of Atomic and Solid State Physics, Cornell University, New York, New York 14853

S. A. Vitiello and L. Reatto
Dipartimento di Fisica, Università degli Studi Milano, 20133 Milano, Italy

G. V. Chester and M. H. Kalos
Laboratory of Atomic and Solid State, Physics and Cornell Theory Center, Cornell University, Ithaca, New York 14853
(Received 17 December 1993; revised manuscript received 27 May 1994)

A trial shadow wave function is introduced to describe the ground state of ^{4}He in the solid and liquid phases. We have used Monte Carlo integration to optimize the parameters of this function, and have carried out a thorough analysis of the shadow description of the system. This shows improved pair correlations, an improved condensate fraction, substantially reduced variational energies, and a good equation of state. We have explored the melting and freezing transition, and find the transition densities to be in good agreement with the exact results of Green's function Monte Carlo (GFMC) calculations. We introduce a second shadow wave function in which a basis set expansion is used to optimize the two-particle correlations. This shadow wave function yields pair-correlation functions in excellent agreement with GFMC, as well as a substantial reduction in the variational energies at all densities.

I. INTRODUCTION

Nearly thirty years ago McMillan[1] published the numerically accurate variational calculation of the ground-state properties of liquid and solid ^{4}He. Since that time many improvements have been made both in the form of variational trial functions and in computational methodologies. The purpose of this paper is to present results for the properties of liquid and solid helium for a class of variational functions that we recently introduced—the "shadow" functions.[2] It is not our primary intention to show that these functions can yield results that are markedly better than any achieved previously, although some are. Rather we aim to show that this class of functions can give a very good systematic description of the homogeneous phases of ^{4}He. We already have achieved some success in applying the shadow wave-function formalism to the roton[3] and vortex[4] states, the liquid solid interface,[5] and helium droplets.[6] Thus our approach seems to be able to deal successfully with inhomogeneous and excited states of helium systems. Encouraged by these results, we return here to establish how well shadow wave functions can describe the homogeneous liquid and solid phases.

Our earliest work with these functions was intended primarily to show that they could describe a crystalline system, and was therefore largely confined to the solid phase. We have now improved the original function and extended the work to four densities in the fluid phase, computing a wide range of physical properties.

Until the introduction of shadow form wave functions variational wave functions for the ground state of ^{4}He took quite different functional forms to describe the solid and liquid phases. In the most common wave function, the Nosanow-Jastrow form,[7] the crystalline order of the solid phase is imposed through one-body terms that explicitly localize the atoms in the vicinity of the lattice sites of a perfect lattice. Such one-body terms violate both the translational symmetry of the Hamiltonian and the permutation (Bose) symmetry of the wave function. Some consideration has been given[8] to wave functions in which the one-body terms have the periodicity of the assumed crystalline phase so that the Bose permutation symmetry is maintained but not the translational symmetry. These forms are certainly acceptable trial functions. However there are good reasons to try to construct a wave function in which the crystalline order arises from the interparticle correlations and does not have to be imposed *a priori*. First the probability distribution corresponding to such a function is the natural quantum analog of the Gibbs distribution which describes a classical crystal. Second it allows one to investigate the phenomena of nucleation of the crystal phase from a fluid phase. Finally a function of this structure is essential if we wish to study phenomena such as vacancy formation, the liquid-solid interface or the formation of metastable amorphous states. However we think it is important to establish the properties of the wave function in the homogeneous fluid and solid phases before proceeding to investigate these more complex phenomena in detail.

The introduction of the shadow form of wave function[2] provided a means of avoiding the introduction of *a priori* equilibrium positions. Shadow wave functions use the fact that simple Jastrow functions can be used to describe systems with crystalline order as was shown long ago by McMillan.[1] Although translationally invariant and Bose symmetric, such Jastrow crystals correspond only poorly with solid ^{4}He. First they share with classical systems a much greater particle localization than is seen in quan-

0163-1829/94/50(18)/13577(17)/$06.00

tum solids and second they have very high energies. In the shadow form, a Jastrow-style crystalline order arises from a set of auxiliary variables, and is thence transferred to the system of real particles by coupling each real particle through a Gaussian factor to one auxiliary variable. These auxiliary, or shadow, variables are finally integrated out. In this way the real particles can have a rather large motion about their equilibrium positions, while the long-range order is preserved.

The original shadow wave function used simple power-law forms for the pseudopotential of the shadow particles. Vitiello *et al.*[9] showed that while such a wave function yields variational energies substantially below those of simple Jastrow wave functions in the liquid phase, its description of the solid phase is in even closer agreement with exact simulation results. Thus, although shadow functions succeeded in offering for the first time a unified picture of both phases of ground state ^{4}He, there was a marked disparity in the success of the description of the two phases, which suggested that the resulting melting-freezing transition would bear little correspondence with that of real helium systems. Reatto and Masserini[10] suggested on the basis of an interpretation of the modulus squared of the shadow wave function as an approximation to the discretized path-integral representation of the density matrix that a more appropriate form of intershadow pseudopotential should contain attractive correlations, and that a scaled form of the helium interaction potential would be appropriate.

We have adopted this suggestion and have carried out an optimization of the parameters of the shadow wave function over a range of densities in both the liquid and solid phases. With this five-parameter wave function we achieved a significant lowering of the energies. From these results we fitted equations of state using a polynomial form for the energy dependence upon density. This yielded melting and freezing transition densities which are in good agreement with those computed from the exact Green's function Monte Carlo (GFMC) method. The structure factor and pair-correlation functions of the shadow form were computed and compared with those of the old form. The condensate fraction n_0 was computed and compared with the original values. Our values for n_0 are now much closer to the best GFMC estimate at both the equilibrium and freezing densities.

In a second form of shadow wave function that we introduce, we have used a more general form for the real interparticle pseudopotential obtained from the basis-set expansion introduced by Vitiello and Schmidt.[11] This also produced a quantitative improvement in our description of liquid and solid phases of helium, although now the wave function contains 13 parameters.

II. AN IMPROVED SHADOW WAVE FUNCTION

The Hamiltonian of the system of N helium atoms in a volume V is

$$H=-\frac{\hbar^2}{2m}\sum_{i=1}^{N}\nabla_i^2+\sum_{i<j}V_A(r_{ij})\ , \tag{1}$$

where the two-body potential $V_A(r)$ is that of Aziz *et al.*[12] This potential was chosen because the significant body of both GFMC and variational work done with it provides useful comparisons. The GFMC work shows that it provides an accurate description of the liquid and solid phase of ^{4}He. Three-body terms in the real potential are believed to introduce only small ($\approx 0.1-0.2$ K) corrections to the energy per particle[13] in the liquid phase, making a somewhat larger contribution in the solid phase. The Aziz potential is given by[12]

$$V_A(r)=\epsilon\left\{A\exp\left[\frac{-\alpha r}{r_m}\right]-\left[C_6\left[\frac{r_m}{r}\right]^6+C_8\left[\frac{r_m}{r}\right]^8+C_{10}\left[\frac{r_m}{r}\right]^{10}\right]F(r)\right\}\ , \tag{2}$$

where

$$F(r)=\begin{cases}\exp\left[-\left[\dfrac{Dr_m}{r}-1\right]^2\right]\ , & \dfrac{r}{r_m}\le D\\ 1\ , & \dfrac{r}{r_m}>D\ .\end{cases}$$

The values of the constants are

$$A=0.544\,850\,4\times10^6\ ,\quad \epsilon/k_B=10.8\ \text{K}\ ,$$
$$\alpha=13.353\,384\ ,\quad C_6=1.373\,241\,2\ ,$$
$$D=1.241\,314\ ,\quad C_8=0.425\,378\,5\ ,$$
$$r_m=2.9673\ \text{Å}\ ,\quad C_{10}=0.178\,100\ .$$

A trial shadow wave function for a system of N Bose particles has the form

$$\Psi_T(R)=\int K(R,S)\psi_s(S)dS\ , \tag{3}$$

where $R\equiv\{\mathbf{r}_1,\mathbf{r}_2,\ldots,\mathbf{r}_n\}$ and $S\equiv\{\mathbf{s}_1,\mathbf{s}_2,\ldots,\mathbf{s}_N\}$. We chose the kernel $K(R,S)$ to have the simple form

$$K(R,S)=\psi_r(R)\prod_k\theta(\mathbf{r}_k-\mathbf{s}_k)\ . \tag{4}$$

The function θ which provides the coupling between the auxiliary, or shadow variables S and the particle variables R is taken to be

$$\theta(\mathbf{r}_k-\mathbf{s}_k)=e^{-C|\mathbf{r}_k-\mathbf{s}_k|^2}\ . \tag{5}$$

C is a variational parameter that we refer to as the interaction strength.

The functions $\psi_r(R)$ and $\psi_s(S)$, which are taken to have the Jastrow form, correlate, respectively, the particles and the shadows. Taken by themselves as variational functions, Jastrow trial functions do not provide good descriptions of the ^{4}He solid phase,[1] since they describe a solid phase in which particles possess the much greater localization than that which typifies classical solids. This contrasts markedly with the diffuse structure seen in solid ^{4}He. Although in the solid phase the system of shadow

particles has the greater structure of a Jastrow solid, the Gaussian coupling of the real particles to the shadow system allows the real particles to be substantially less structured.

In the earlier work, both of the functions $\psi_r(R)$ and $\psi_s(S)$ were chosen to have a pseudopotential of the same power-law form that was used by McMillan.[1] For $\psi_s(S)$ we now use a Jastrow function

$$\psi_s(S)=\prod_{i<j} e^{-w(s_{ij})}, \tag{6}$$

where $w(s)=\delta V_A(\alpha s)$. That is, the pseudopotential is taken as a rescaled version of the physical two-body potential $V_A(r)$. Here δ and α are the variational parameters.

While there are phenomenological motivations for relating $w(s)$ to V_A, the following argument provides a good theoretical reason for choosing an attractive pseudopotential like our $w(s)$. A wave function of the shadow form with a pseudopotential directly related to V_A is suggested by the following argument. Consider the discretized path-integral representation of the density matrix of the system.[14] The action for a path is the integrated sum of kinetic and potential energies as the system follows that path in imaginary time. An integration over the endpoints of these paths may be transformed into an integration over the centers of mass of the paths.[15] In the shadow wave function, the auxiliary variables can be thought of as corresponding to these centers of mass of the particle paths. The Gaussian coupling of a particle to its auxiliary variable results in a diminished contribution of widely diffuse paths to the wave function. Interactions between different particles at particular instants of imaginary time are replaced in part by an interaction between the centers of mass of their paths. This interaction between mass centers mimics the interactions in a system of particles, and provides further justification of our use of the term shadow "particle" to describe this "secondary" system. Finally, the fact that the source of this interaction is the potential between helium atoms suggests that one use a parametrized form of the He-He potential as the pseudopotential between the shadow particles. This analogy is most appealing in the dense fluid and solid phases, where because of the hard core of the atomic potential the particle paths may be thought of as being reasonably confined by surrounding particles. The form we have used for $w(s)$ was suggested by Reatto and Masserini[10] as a simple check of this hypothesis.

The present work also explores two Jastrow forms for $\psi_r(R)$. In the first one, this function was chosen to have a pseudopotential of the McMillan fifth power-law form:

$$\psi_r(R)=\prod_{i<j} e^{-(1/2)u(r_{ij})},$$

where

$$u(r)=\left[\frac{b}{r}\right]^5. \tag{7}$$

Here $r_{ij}=|\mathbf{r}_i-\mathbf{r}_j|$ and b is a variational parameter.[16] This form of shadow wave function will be denoted by $M+A(S)$.

The second form for $\psi(R)$ that we explore arises from the following consideration. To overcome the limitations of the McMillan form for the pseudopotential, an optimized basis set expansion can be introduced[11] that has been shown to describe accurately the two-body correlations in the ground state of ^{4}He systems. We refer to the shadow wave function in which the two-body correlations of $\psi_r(R)$ have been optimized in this way as $O2B+A(S)$.

Both these forms of $\psi_r(R)$ do not have the correct long-range behavior for large interparticle separation.[17] We have not included this in our wave function because this long-range behavior cannot be dealt with by standard Monte-Carlo techniques. We also know that its inclusion will lead to only a very small change in the energy of the system.[18]

We will compare the results we obtain from the $M+A(S)$ and $O2B+A(S)$ forms for the shadow wave function with those found by Vitiello *et al.*;[9] we refer to this wave function as $M+M(S)$. In their trial shadow function both of the pseudopotentials, for the particles and for the shadow variables, have the McMillan form.

III. THE VARIATIONAL CALCULATION

The variational energy is given by

$$E_T=\frac{\int dR\,\Psi_T H\Psi_T}{\int dR\,|\Psi_T|^2}, \tag{8}$$

which is the sum of the kinetic energy E_K and of the potential energy E_V. Because the variational energy possesses a smaller variance when evaluated using the Pandharipande-Bethe[19] form for the kinetic energy, this form was used in our calculations:

$$E_K=-\frac{\hbar^2}{2m}\frac{\int dR\,\Psi_T\sum_{i=1}^{N}\nabla_i^2\Psi_T}{\int dR\,|\Psi_T|^2}. \tag{9}$$

The potential energy is given by

$$E_V=\frac{\int dR\,\Psi_T\sum_{i<j}V_A(r_{ij})\Psi_T}{\int dR\,|\Psi_T|^2}. \tag{10}$$

The variational expectation value of an operator O can be written as

$$\langle O\rangle=\int\int\int dR\,dS\,dS'p(R,S,S')\times\left\{\frac{O\psi(R)\prod_k\theta(\mathbf{r}_k-\mathbf{s}'_k)}{\psi(R)\prod_k\theta(\mathbf{r}_k-\mathbf{s}'_k)}\right\}, \tag{11}$$

since O acts only upon the variables describing the system of real particles. $\langle\ \rangle$ denotes an average with respect to $|\Psi_T(R)|^2$. Here,

$$p(R,S,S')=\frac{\psi_r(R)^2\left[\prod_k\theta(\mathbf{r}_k-\mathbf{s}_k)\psi_s(S)\right]\left[\prod_k\theta(\mathbf{r}_k-\mathbf{s}'_k)\psi_s(S')\right]}{\int\int\int dR\,dS\,dS'\psi_r(R)^2\left[\prod_k\theta(\mathbf{r}_k-\mathbf{s}_k)\psi_s(S)\right]\left[\prod_k\theta(\mathbf{r}_k-\mathbf{s}'_k)\psi_s(S')\right]}\ . \tag{12}$$

To evaluate the expectation value of O the Metropolis algorithm is used to sample the probability density $p(R,S,S')$ from the $9N$ dimensional configuration space of the system coordinates together with the two sets of shadow coordinates. The details of this procedure are the same as those used by Vitiello *et al.*[9] It is interesting to note that $p(R,S,S')$ is equivalent to the Boltzman factor of a system of classical trimers at some effective temperature, where a trimer consists of a particle interacting harmonically with two shadow particles, one from each of the two sets S and S'. This is illustrated in Fig. 1. There is no direct interaction between the two distinct shadows of a given trimer. Rather, they interact with one another indirectly through their interaction with the real particles and by the interaction between trimers. Because this analogous classical system consists of trimers, with a very unusual interaction, results are not easily extracted by analyzing this classical system.

In addition to the kinetic, potential, and total energies we have also computed the radial distribution function

$$g(r)=\frac{1}{N\rho}\sum_{i\neq j}\langle\delta(|\mathbf{r}_i-\mathbf{r}_j-\mathbf{r}|)\rangle\ , \tag{13}$$

and the structure function

$$S(\mathbf{k})=\frac{1}{N}\langle\rho_{\mathbf{k}}^{\dagger}\rho_{\mathbf{k}}\rangle\ , \tag{14}$$

where ρ is the particle density and $\rho_{\mathbf{k}}$ is given by $\rho_{\mathbf{k}}=\sum_j e^{-i\mathbf{k}\cdot\mathbf{r}_j}$.

A further probe of the trial wave function is the condensate fraction n_0, which is the fraction of particles occupying the zero momentum state. This quantity is expressible in terms of $\rho_1(r)$, the off-diagonal matrix element of the one-body density matrix ρ_1:

$$\rho_1(r)=\langle\mathbf{r}|\rho_1|0\rangle=\left\langle\frac{\Psi_T(\mathbf{r}_1,\mathbf{r}_2,\ldots,\mathbf{r}_i+\mathbf{r},\ldots,\mathbf{r}_N)}{\Psi_T(\mathbf{r}_1,\mathbf{r}_2,\ldots,\mathbf{r}_i,\ldots,\mathbf{r}_N)}\right\rangle\ ,$$

where the average is taken with respect to $|\Psi_T|^2$. For a shadow form wave function, $\rho_1(r)$ may be expressed as

$$\rho_1(r)=\left\langle\frac{\psi_r(R')\prod_k\theta(\mathbf{r}'_k-\mathbf{s}_k)}{\psi_r(R)\prod_k\theta(\mathbf{r}_k-\mathbf{s}_k)}\right\rangle\ , \tag{15}$$

where $R'=\{\mathbf{r}_1,\ldots,\mathbf{r}_i+\mathbf{r},\ldots,\mathbf{r}_N\}$, and where R and S are as in (3). In terms of $\rho_1(r)$ the condensate fraction is given by[20]

$$n_0=\lim_{r\to\infty}\rho_1(r)\ . \tag{16}$$

The condensate fraction provides a very different assessment of a trial wave function. In practice a wave function yielding good variational energies may not show corresponding success in describing the off-diagonal long-range order represented by the asymptotic form of the one-body density matrix. Conversely, a good condensate fraction does not imply good variational energies, as the variational energy is very insensitive to the asymptotic form of $\rho_1(r)$.

All our computations start from an ordered initial configuration corresponding to an fcc crystal. When the density of the system is below a certain value (approximately $\rho\sigma^3=0.43$), it quickly evolves to a disordered fluid state. This is shown very clearly by monitoring the value of $S(k)$ at a reciprocal-lattice vector and the value of the mean-square displacements of the particles from their initial positions. $S(k)$ at a reciprocal-lattice vector drops rapidly from a value in the range of 30–50 to a value of the order of unity. The mean-square displacement rapidly grows until it has reached a maximum value proportional to the linear dimension of the simulation cell. However at high densities ($\rho\sigma^3$ greater than 0.492) the evolution is entirely different and the crystal phase is stable throughout the entire Monte Carlo simulation. However this crystalline order is not an artifact of the initial state. We have recently[21] been able to demonstrate in three dimensions the spontaneous nucleation of the crystalline phase, when the system is started from a completely disordered initial configuration. In the work reported in this paper we chose the initial configuration to be that of an fcc lattice as a matter of convenience.

When optimizing the variational parameters, it proved useful to use a reweighting scheme,[22] which allowed the comparison of the variational energies for two sets of slightly different parameters. Such a procedure is espe-

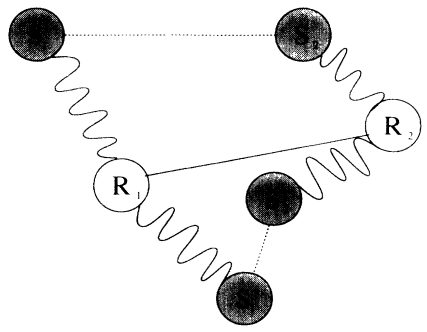

FIG. 1. The figure shows two of the classical trimers which arise when the Metropolis algorithm is used to sample the modulus squared of the shadow wave function. The continuous line represents the real particle pseudopotential $u(r)$ and the dotted lines that of the shadows, $w(s)$. The labels on each monomer designate the system to which that monomer belongs, either the real or one of the two shadow sets.

cially useful when the energy differences are much smaller than the statistical variation of separate energy estimates. As our variational search progressed, it became apparent that steps in the Metropolis random walk are correlated over longer times with our $M+A(S)$ (typically ≈ 1500 passes in the liquid phase) form than they were with the $M+M(S)$ form (several hundred passes). The wave function with an attractive pseudopotential for the shadow particles shows markedly enhanced pair correlations between the shadow variables, and to a lesser extent between the real variables. It is likely that these enhanced correlations are the source of the longer correlation and equilibration times observed in our runs.

Our runs consisted of a total of about 112 000 passes during each of which an attempt was made to move every particle and shadow coordinate. In both the liquid and solid phases, the initial configuration for the system is a perfect fcc lattice. In the liquid phase, the equilibration is accomplished in two steps. The initial configuration is run for 400 passes using a simple Jastrow wave function of the McMillan form. The configuration obtained in this way is used as the starting configuration for both the real system and the system of shadow coordinates, so that in this starting configuration the shadow particles occupy the same position as their corresponding real particles. The same stage of the equilibration phase is carried out in the usual way, with a number of passes being discarded until the asymptotic regime of the random walk has been reached. We chose to be conservative in this, allowing about 32 000 passes for the equilibration of the $M+A(S)$ runs shown in Table I. This equilibration phase is followed by about 80 000 passes which comprise the equilibrated random walk.

The initial equilibration in the solid phase was carried out in a different way from that of the liquid, since the initial fcc lattice becomes rapidly disordered if a Jastrow wave function of the McMillan form is used to determine its evolution. Once the crystal has become disordered, it will not recrystallize during a typical run of the order of 10^5 passes. Because of this, and also because we want to equilibrate the random walk as rapidly as possible, in the initial equilibration phase of the solid the shadow coordinates are held fixed at the points of an fcc lattice. The real particles, coupled to these fixed shadow coordinates,

TABLE I. The table shows variational (E_T), kinetic (E_K), and potential (E_V) energies obtained from several wave functions. The results labeled $M+A(S)$ are for the shadow wave function with a scaled Aziz shadow pseudopotential. $O2B+A(S)$ refers to a shadow form wave function in which a basis set method has been used to optimize the real two-particle pseudopotential $u(r)$. $M+M(S)$ refers to a shadow wave function using a McMillan form power law pseudo-potential for both the system particles and the auxiliary variables (Ref. 9). In this case the subscript denotes the power of the McMillan form shadow pseudopotential. $O2B+T$ refers to results obtained by Vitiello and Schmidt (Ref. 11). GFMC refers to the Green's function Monte Carlo results of Whitlock and Panoff (Ref. 23). We also show the available experimental data (Ref. 24).

ρ (Å^{-3})		E_T	E_K	E_V
0.0196				
	$M+A(S)$	−6.561±0.032	11.854±0.042	−18.415±0.019
	$O2B+A(S)$	−6.695±0.027	12.761±0.033	−19.456+00.013
	$O2B+T$	−6.804±0.015		
	GFMC[a]	−7.03±0.04	12.08±0.08	−19.11±0.07
0.0218				
	$M+A(S)$	−6.599±0.034	14.085±0.045	−20.684±0.024
	$O2B+A(S)$	−6.789±0.023	14.889±0.042	−21.679±0.024
	$M+M(S)_{n=9}$	−6.165±0.019	14.420±0.021	−20.586±0.014
	$O2B+T$	−6.862±0.016	14.468±0.52	−21.331±0.048
	GFMC	−7.12±0.02	14.47±0.09	−21.59±0.09
	Experiment	−7.14		
0.0240				
	$M+A(S)$	−6.398±0.019	17.171±0.021	−23.569±0.018
	$O2B+A(S)$	−6.615±0.029	17.738±0.040	−24.353±0.023
	$O2B+T$	−6.524±0.020		
	GFMC	−6.89±0.05	17.3±0.1	−24.21±0.09
	Experiment	−7.00		
0.0262				
	$M+A(S)$	−5.871±0.016	20.133±0.021	−26.008±0.020
	$O2B+A(S)$	−6.286±0.022	20.508±0.035	−26.794±0.022
	$M+M(S)_{n=5}$	−5.342±0.012	19.339±0.038	−24.681±0.039
	$O2B+T$	−5.837±0.023		
	GFMC	−6.56±0.06	20.1±0.2	−26.7±0.1
	Experiment	−6.53		

[a]The GFMC result is for $\rho=0.0197$ Å^{-3}.

evolve for several hundred passes by a series of Metropolis steps in which the variational parameters are taken as slightly different from the optimum ones to assure high mobility. In this way the real particles remain in the vicinity of their crystal lattice sites because of their Gaussian coupling to the fixed coordinates. Next, as in the second equilibration phase of the liquid, the shadow particles are freed and the equilibration continues for about 25 000 passes. After the two equilibration phases the equilibrated random walk continues for 80 000 passes. This procedure results in a more rapid equilibration than a direct relaxation from an initial lattice. However, we have verified that a direct relaxation from an initial lattice yields the same equilibrium results.

It should be noticed that this equilibration procedure for the solid is equivalent to using, during the first phase, a Jastrow-Nosanow function in place of the shadow function. In fact a Jastrow-Nosanow function ($\Psi_{JN}(R)$) has the form[7]

$$\Psi_{JN}(R)=\Psi(R)\prod_k \theta(\mathbf{r}_k-\mathbf{R}_k^0)\ , \tag{17}$$

where $\Psi(R)$ is a Jastrow function, θ is a Gaussian, and $\{\mathbf{R}_k^0\}$ are the positions of the lattice sites of the crystal. It is clear that, once normalized, this function is equivalent to Eq. (3) when $\bar{s}_k=\bar{R}_k^0$. This also shows that (17) is a special case of (3): this form is appropriate when the shadow pseudopotential in $\Psi_s(S)$ is so strong that the shadows cannot move. The rigid lattice of shadows means that correlations between helium atoms are instantaneously transmitted across the system in the solid phase and this is embodied in Eq. (17). On the other hand with a shadow pseudopotential of finite strength only local correlations are effective and this is the essential difference between our wave function and the Jastrow-Nosanow function.

IV. RESULTS FOR THE FLUID PHASE

The organization of our fluid phase results is as follows. First we make comparisons between the variational energies of our wave function and those of GFMC and experiment. The same comparisons are then made with the original $M+M(S)$ form of shadow wave function and with two other variational forms from the literature. The radial distribution functions of our forms are compared with those of the earlier shadow wave function and with GFMC. Comparisons are then made between the variational structure functions, experiment and GFMC. Finally, our variational results for the condensate fraction are presented. Table II shows the values of the optimum variational parameters b, C, α, and δ for the $M+A(S)$ wave function in the liquid phase.

TABLE II. The table shows the optimum parameters for the liquid phase of the $M+A(S)$ form wave function.

ρ (Å^{-3})	b (Å)	C (Å^{-2})	δ (K^{-1})	α
0.0196	2.812	0.8419	0.088	0.915
0.0218	2.812	0.8419	0.095	0.915
0.0240	2.837	0.9184	0.105	0.920
0.0262	2.837	0.9031	0.110	0.910

A. Energy

Table I shows the energy per particle obtained from our $M+A(S)$ and $O2B+A(S)$ forms of trial functions. The kinetic and potential energies are also shown. Our simulations were carried out on systems of 108 and 256 particles. Also included in the table are several results from the literature. $O2B+T$ designates variational energies obtained using a trial wave function with optimized two-body and triplet correlations.[11] Energies obtained with a shadow wave function having a pure repulsive pseudopotential of the McMillan form for both the real particles and the shadows[9] are designated by $M+M(S)$. Finally, we show the GFMC energy and the corresponding kinetic and potential energies from the liquid phase work of Whitlock and Panoff[23] for systems of 64 particles, as well as the experimental energies of Roach, Ketterson, and Woo.[24]

1. *Comparisons of $M+A(S)$ with GFMC and experiment*

The GFMC energies were obtained by a Monte Carlo solution of Schroedinger's equation. They are believed to be exact for the Aziz potential apart from small statistical uncertainties. Our $M+A(S)$ variational energies are consistently about 0.5 K above the GFMC energies at all densities in the liquid phase except at the GFMC freezing density 0.0262 Å^{-3}. At that density our energy is about 0.7 K above the GFMC result. Our wave function yields a lower kinetic energy compared with GFMC at all except the freezing density. The difference in our $M+A(S)$ kinetic energies and those of GFMC is most pronounced at low densities and less so as the density increases. At the freezing density the two results are in agreement. The variational potential energy is consistently higher by about 0.7 K than the GFMC potential energy, except at the equilibrium density where it is about 0.9 K higher. Overall our variational results are above those of GFMC by an amount essentially independent of the density except for the small variation seen near the freezing density.

Table I also shows experimental energies derived from the results of Roach, Ketterson, and Woo.[24] Because of the close agreement of GFMC with experiment, essentially the same observations arise from the comparison of our energies with experiment as with GFMC.

2. *Comparison of $M+A(S)$ with the $M+M(S)$ shadow wave function results*

A comparison of the energies of the $M+A(S)$ form with the results obtained using a repulsive power-law form for the shadow pseudopotential is made at the equilibrium and freezing densities. These are the only two densities in the liquid phase where that function was optimized. This comparison shows the improvement in this form over the original shadow form.

At the equilibrium density, our form yields a variation-

al energy 0.5 K lower than that with the repulsive shadow pseudopotential. This is a substantial improvement when one considers that the $M+M(S)$ energy is only about 1 K above the GFMC result. At the freezing density, the reduction in energy is about 0.5 K. A good illustration of the significant improvement in our $M+A(S)$ form over $M+M(S)$ is that the reduction in energy is nearly half of the difference between the $M+M(S)$ and GFMC. The improvement is comparable to the reduction in energy which occurs when explicit three-particle correlations are introduced into the wave function.[25]

3. *The basis-set method*

As we mentioned in Sec. II, a method has recently been introduced[11] to describe the two-body correlations between helium atoms in a many-body wave function. The many-body correlations are written in the usual way as a product of two-body factors $f(|\mathbf{r}_{ij}|)$. The two-body correlation function $f(r)$ is then expanded in terms of a basis set $f_n(r)$,

$$f(r)=\sum_n c_n f_n(r)$$

subject to

$$\sum_n c_n = 1 \ .$$

The $f_n(r)$ are chosen to be the set of functions which are solutions of the two-body Schroedinger equation for a pair of helium atoms interacting via the Aziz potential, subject to the boundary condition that $f_n(r>d)=1$. The parameter d was chosen to be one-half the size of the simulation cell. Schmidt and Vitiello[11] truncated this expansion at ten terms and then optimized the variational energy with respect to the ten coefficients in the expansion. The resulting energies were, when triplet correlations were also included, lower than previous variational estimates at all densities in the fluid phase. This form is referred to as $O2B+T$.

To apply this method within the framework of our shadow wave function, we replaced the simple McMillan form for the two-body correlation function for the real particles with an expansion in terms of the same ten basis functions as were used by Schmidt and Vitiello. We then held the parameters describing the shadow correlations fixed and minimized with respect to these ten parameters. The shadow wave function having this form is called the $O2B+A(S)$ form. With this approach we were able to lower the ground-state energy at all densities in the fluid phase. Full minimization would require that also the shadow parameters of the $O2B+A(S)$ form were reoptimized. Computation in few cases showed that the energy was not significantly lowered by this. A difficulty which arises in the optimization of the $O2B+A(S)$ parameters is due to the insensitivity of the variational energy to the long-range behavior of $u(r)$. As a result of this insensitivity, several different sets of variational parameters $\{c_i\}$ can yield essentially the same energies, even when there are qualitative and quantitative differences in the long-range behavior of the different pseudopotentials.

We show the $O2B+A(S)$ energies at four densities in the fluid phase in Fig. 2(a). In the same figure we display the energies using our $M+A(S)$ shadow wave function, as well as those obtained by Schmidt and Vitiello's $O2B+T$ form. Also included are results obtained by the GFMC method. The smooth curves shown there are third-degree polynomial fits to the data. These fits are described in detail in Sec. IV B.

While the basis-set approach leads to lower energies the energy density curve is now comparatively flat, i.e., rises much less steeply as the volume decreases. This implies that the pressure, which is simply the negative of the slope of the energy curve with respect to volume, is much too low in the high density fluid. This is shown in Fig. 2(b). We therefore have a somewhat paradoxical result; the energies are lower but the equation of state $p(\rho)$ is unsatisfactory. It is possible that a resolution of this paradox might be found in a further minimization of the coefficients in the basis-set expansion. In other words, there may be another region of parameter space which leads to low energies and also to a satisfactory equation of state. Since the main focus of this work is to examine the consequences of introducing attractive correlations between the shadow particles, we have not undertaken

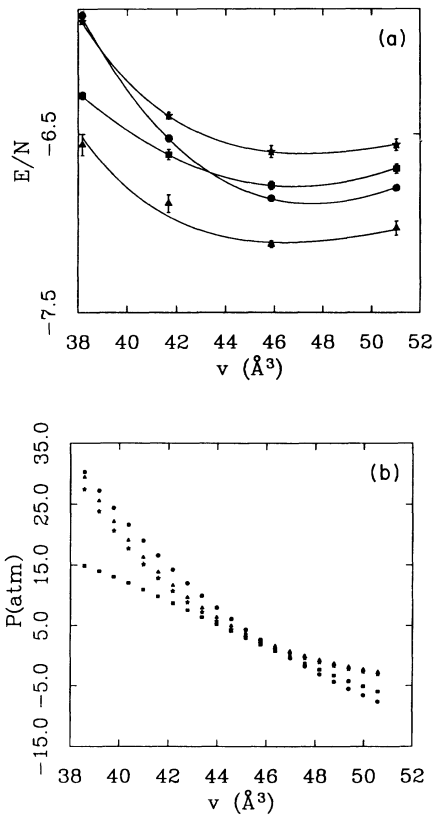

FIG. 2. (a) The figure shows our $O2B+A(S)$ variational energies, together with those of Vitiello and Schmidt. The GFMC energies are also shown (Ref. 23). The smooth curves are a polynomial fit to the energies. Squares denote $O2B+A(S)$, circles $O2B+T$, triangles GFMC, and stars $M+A(S)$. (b) This figure shows the pressure as a function of specific volume obtained by differentiating the smooth curves of (a). The symbols are as in (a).

the rather formidable task of making a still wider search in the parameter space for the real particle correlations.

4. Comparison of the $M+A(S)$ form with $O2B+T$

It is interesting to compare the energies obtained from our $M+A(S)$ form with those from the $O2B+T$ form[11] of Vitiello and Schmidt. Our form shows a steady improvement compared with the $O2B+T$ form as the density increases. Although it gives a variational energy about 0.2 K higher than that of the $O2B+T$ form at the lowest density studied, this energy difference decreases at higher densities until at the freezing density the energies of the two wave functions are in agreement. Because our trial function compares well with a wave function having both two- and three-body correlations, it is evident that this form of the shadow function recovers a large part of the energy which is due to correlations between more than two atoms.

5. Comparison of $O2B+A(S)$ with other variational results

The results for the $O2B+A(S)$ shadow wave function illustrate the improvement in the shadow description when a much more general form for the real particle pair correlations is used. Comparison of the $O2B+A(S)$ energies with those of the $M+A(S)$ form shows that the former leads to a decrease of about 0.14 K compared with the latter at the lowest density. The trend as a function of density is for the $O2B+A(S)$ form to improve until at the highest density studied in the liquid phase it yields an energy which is 0.4 K lower than that of the $M+A(S)$ form. This means that the $O2B+A(S)$ wave function yields a variational energy almost a full degree lower than that of the original $M+M(S)$ shadow wave function.

Thus, the optimization of the two-body correlations gives rise to a significant improvement in the variational energy near the freezing density, whereas the corresponding improvement near the equilibrium density is less than half as great, and is less still at the lowest density considered. The improvement with density of the $O2B+A(S)$ form compared with the $M+A(S)$ form is expected from the fact that at higher densities, the particles probe the inner region of the potential more frequently than at lower densities. Thus, the wave function which represents the correct two-particle correlations in this inner region most correctly should show the greatest improvement at higher densities. In contrast with the pair-correlation functions computed from the basis-set expansion, the McMillan form Jastrow function of the $M+A(S)$ form is *a priori* inappropriate for the inner regions of the Aziz potential. Another possibility, mentioned previously, is that the arduous variational search for the coefficients in the basis-set expansion may have been incomplete, so that there may be other regions of the parameter space that yield even lower variational energies. Even considering this possibility, our new results at the freezing density are the lowest variational energies reported using variational Monte Carlo.

B. The equation of state

Our energies at four densities in the fluid phase were fitted to a third-degree polynomial of the form

$$\frac{E}{N}=A+B\left[\frac{\rho-\rho_0}{\rho_0}\right]^2+C\left[\frac{\rho-\rho_0}{\rho_0}\right]^3.$$

The parameter ρ_0 is the zero pressure, or equilibrium density. Such a form[24] describes very well the experimental equation of state, and has widespread use in the variational and GFMC literature. The values of the parameters in the fit and their errors are shown in Table III. The errors shown there arise from the statistical uncertainty in the energies. The GFMC parameter values reported by Kalos *et al.*[13] are also shown in the table. The values of the curvature terms B and C show the extent to which the variation with density of our variational result agrees with that of the GFMC calculation.

The table shows that the coefficients B, C, and ρ_0 for the $M+A(S)$ form are in good agreement with the GFMC values. Because of the agreement, the pressure, given by $\rho^2[\partial E(\rho)/\partial\rho]$, is well represented by the $M+A(S)$ form. The table illustrates the discrepancy between the $O2B+A(S)$ and GFMC equation of state remarked upon previously, which is unambiguous even considering the rather large uncertainties in the fit.

C. The radial distribution function

Figures 3(a) and 4 show the radial distribution functions $g(r)$ obtained in the liquid phase at the equilibrium and freezing densities. These results are shown for our $M+A(S)$ and $O2B+A(S)$ forms, together with those of the $M+M(S)$ shadow wave function and the GFMC results of Kalos *et al.*[13] At the equilibrium density, the original $M+M(S)$ form wave function yielded a $g(r)$

TABLE III. Fitting coefficients in the equation of state curve in the liquid phase for the $M+A(S)$ and $O2B+A(S)$ variational results. The GFMC result of Kalos *et al.* (Ref. 13) is also shown. Our energies at four densities in the fluid phase were fitted to a third-degree polynomial of the form $E/N=A+B[(\rho-\rho_0)/\rho_0]^2+C[(\rho-\rho_0)/\rho_0]^3$.

	$M+A(S)$	$O2B+A(S)$	GFMC
A	-6.610 ± 0.036	-6.796 ± 0.025	-7.110 ± 0.023
B	10.3 ± 5.5	14.10 ± 4.18	10.08 ± 3.2
C	11.3 ± 18.5	-18.7 ± 18.1	12.59 ± 8.5
ρ_0 (Å^{-3})	$0.021\,17\pm0.000\,26$	$0.021\,36\pm0.000\,19$	$0.021\,56\pm0.000\,29$

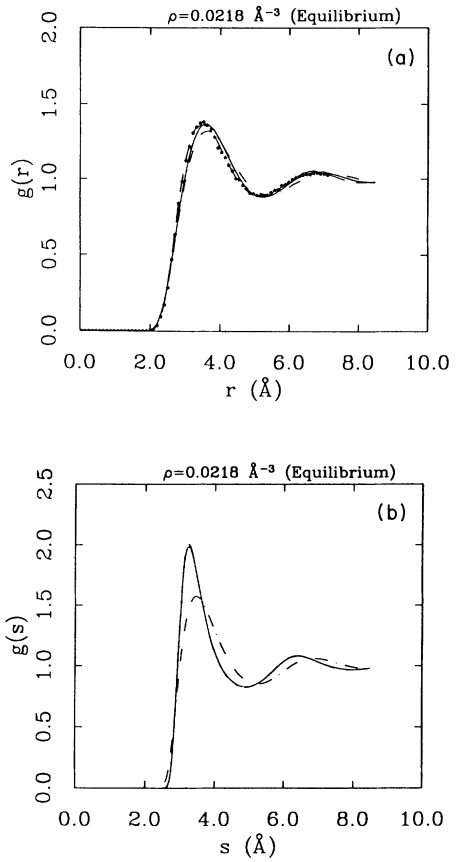

FIG. 3. (a) and (b) These curves show the pair-correlation functions of the real and shadow systems, respectively, at the equilibrium density, for both our $M+A(S)$ and $O2B+A(S)$ forms and for the early $M+M(S)$ shadow function. The continuous curve denotes $M+A(S)$, the dashed curve $O2B+A(S)$, and dash-dot $M+M(S)$. The GFMC curve is denoted by stars. In (b), the $M+A(S)$ and $O2B+A(S)$ results are barely distinguishable.

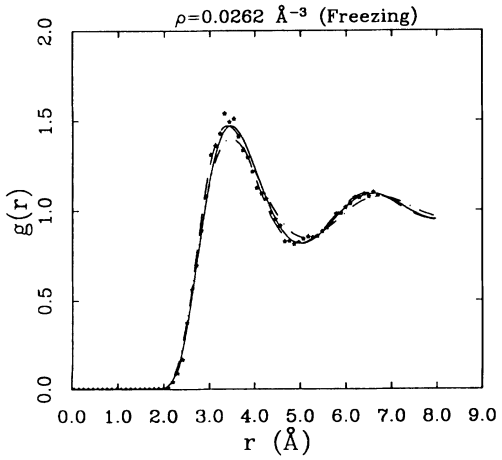

FIG. 4. This figure shows the pair-correlation function at freezing. The smooth curve denotes $M+A(S)$, dashes denote $O2B+A(S)$, and dash-dot denotes $M+M(S)$. The stars denote GFMC.

which differed from GFMC chiefly in that it predicted a diminished nearest-neighbor maximum by about 0.08, at a value of r about 0.1 Å larger than the maximum of the GFMC curve. The entire curve appeared shifted to larger values of r compared to the GFMC curve by this amount. Our form improves over the $M+M(S)$ form by showing an enhanced nearest-neighbor presence, so that the nearest-neighbor maximum of $g(r)$ is only about 0.015 smaller than the GFMC result. The curve is still shifted compared with the GFMC result by nearly the same amount as the $M+M(S)$ curve. We conjecture that this shift is an artifact of the fifth power-law form for the pseudopotential $u(r)$, which is present in both trial functions. This conjecture appears substantiated by the observation that in the $O2B+A(S)$ form with optimized two-particle correlations, no such shift is seen. The $OB+A(S)$ curve is in excellent agreement with GFMC.

The trend seen at the equilibrium density in Fig. 3(a) is repeated in Fig. 4 at the freezing density. Statistical errors in the GFMC $g(r)$ near the maximum of $g(r)$ are large, so a detailed comparison with GFMC is not possible here. The $M+M(S)$ curve is again shifted with respect to the GFMC curve, and shows a smaller nearest-neighbor maximum. Our $M+A(S)$ $g(r)$ curve is shifted by the same amount, but shows a larger nearest-neighbor maximum than that of $M+M(S)$ and a smaller one than GFMC. The pair-correlation function of our $O2B+A(S)$ form is again in good agreement with GFMC.

Figure 3(b) shows the radial distribution function $g(s)$ of the shadow particles for the $M+M(S)$ and for our $M+A(S)$ wave function at the equilibrium density. This shows that the primary difference in $g(s)$ is that the nearest-neighbor maximum is substantially higher than in the $M+M(S)$ form. This enhanced shadow particle correlation gives rise to the increased correlation among the real particles that we have just noted. The $g(s)$ for our form compared to the $M+M(S)$ form also is shifted inward to smaller values of s. Earlier work on shadow wave functions[9] showed the shadow particles to be correlated to a greater extent than the real particles, and this result is true to an even greater extent for our shadow wave function. In this sense their correlations are somewhat closer to, thought not as great as, those expected in a classical system. In Fig. 5(a), we show $g(s)$ for the $M+M(s)$ power-law form at the equilibrium density, together with the corresponding shadow correlation factor $f_M(s)$. Figure 5(b) shows $g(s)$ for our form together with $f_A(s)$. Note that in 5(b), $g(s)$ and $f_A(s)$ have coincident maxima, and that the structure of $g(s)$ is similar to that of $f_A(s)$.

D. The structure function

Figures 6(a) and (b) show the structure functions $S(k)$ obtained from our variational calculation and the experimental data. The static structure factor is defined in Eq. (14). The isotropic state structure factor $S(k)$ may also be expressed in terms of the radial distribution function $g(r)$ as

$$S(k)=1+4\pi\rho\int_0^\infty r^2\frac{\sin(kr)}{kr}[g(r)-1]dr\ . \qquad (18)$$

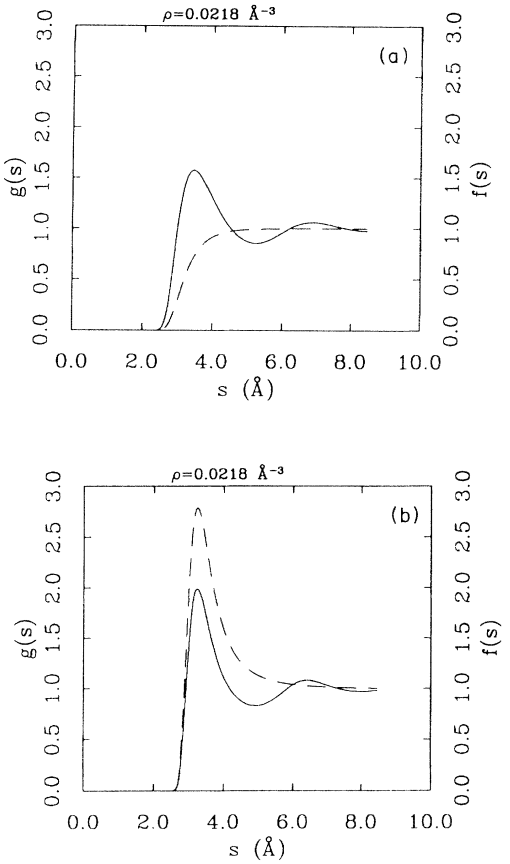

FIG. 5. (a) and (b) These figures show the shadow pair-correlation functions together with the function $f(s)=e^{-w(s)}$, respectively, for both the $M+A(S)$ and $M+M(S)$ forms at equilibrium. The function $w(s)$ is the pair pseudopotential for $\psi_s(S)$. The smooth curves denote $g(s)$, while the dashed line is $f(s)$.

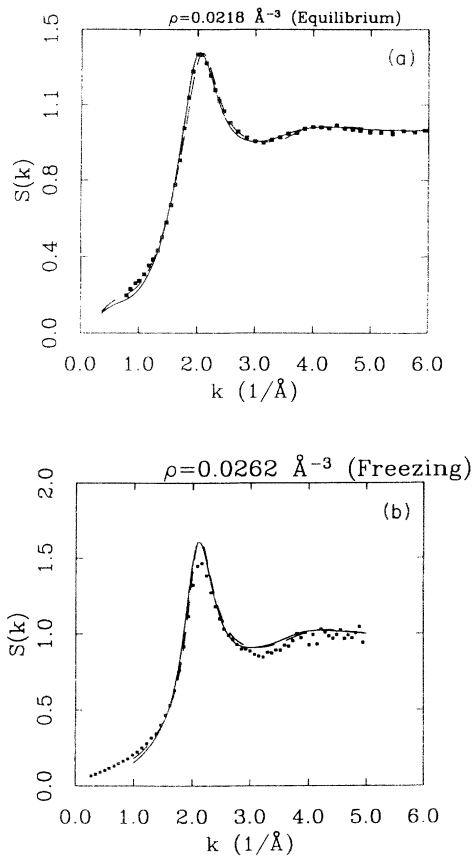

FIG. 6. (a) and (b) The figures show our structure function at the equilibrium and freezing densities, respectively. The smooth curves are $M+A(S)$ results, dashes denote $O2B+A(S)$ and squares denote experimental results.

To determine $S(k)$ from this expression it is necessary to extend the radial distribution function beyond one-half the size of the simulation cell. To accomplish this, a fit was made to $g(r)$ beyond its first maximum using the form

$$g(r)-1=\frac{1}{r}\sum_{n=1}^{3} A_n e^{-z_n r}$$

for complex numbers z_n and real constants A_n.[26] This fit was used to evaluate the integrand in the region outside the simulation cell. As a check on this procedure, Eq. (14) was used to directly compute $S(\mathbf{k})$ during the simulation at the equilibrium density, a procedure which is only possible on the discrete set of $\mathbf{k}$ allowed by the periodic boundary conditions. These results were then compared with the $S(k)$ obtained from Eq. (18). The comparison was made over a range of system sizes from 32 to 256 particles.[27] With increasing system size the discrete $S(\mathbf{k})$ converged to the $S(k)$ curve that was obtained using Eq. (18). The $S(k)$ curves obtained from this equation were in excellent agreement with one another for both the 108 and 256 particle systems.

Figure 6(a) shows $S(k)$ at the equilibrium density 0.0218 Å^{-3}. The experimental $S(k)$ shown in this figure is the result reported by Svensson and co-workers,[28,29] and was obtained by neutron diffraction at saturated vapor pressure at $T=1.0$ K. Figure 6(b) shows $S(k)$ at the freezing density. The experimental curve in that figure is from Wirth and Hallock,[30] and was obtained by x-ray scattering at a density of 0.025 73 Å^{-3} and $T=1.16$ K.

The agreement of the equilibrium variational structure functions of Fig. 6(a) with experiment is seen to be very good. There are a number of reasons why our simulation is not expected to give good agreement with experiment for small k. First, the experiment was carried out at $T=1.0$ K, and although the effect of the finite temperature on the large-k region of $S(k)$ should be minimal, the small-k region is substantially modified by a finite temperature.[17] In addition, our wave function does not contain the proper long-range correlations necessary for the linear behavior of $S(k)$ which is observed in ^{4}He.[17] These correlations do not effect the energy in a significant way,[18] though they are necessary for the proper long-range pair correlations.

The comparison of the $S(k)$ results with the experimental data near the freezing density is shown in Fig. 6(b). It is not as good as that at the equilibrium density.

It is clear from the experimental curve that there is considerable uncertainty in these results for large values of k. Our wave function gives a peak in $S(k)$ which is somewhat larger than experimental data. It should be noted that the experimental curve is obtained at a density slightly different from our freezing density. A rough estimate of the order of the reduction in the peak of $S(k)$ that we expect in the experimental result compared with ours can be obtained by interpolating between the experimental results of Wirth and Hallock[30] at 0.0244 and 0.0257 Å^{-3}. Such an interpolation suggests the experimental $S(k)$ may be reduced by about 1.5% compared with ours due to the slightly differing densities of the two results. The difference in height of our maximum of $S(k)$ at freezing and the experimental result is about 9%. This approximant analysis suggests that the slight difference in density of the two results is alone unable to account for the discrepancy.

E. The condensate fraction

Our method of computing n_0 is more elaborate than that which is normally used. The procedure we use is described in the work of Vitiello *et al.*[9] Briefly, configurations generated by sampling $p(R,S,S')$ [see Eq. (12)] are useful for calculating $\rho_1(r)$ only for small values of r. The reason is that the computation of $\rho_1(r)$ from Eq. (15) for large values of r gives zero for any Monte Carlo run of feasible duration because of the Gaussian coupling of the particles to the shadow variables. This can be seen from the observation that the quantity being averaged in Eq. (15) approaches zero as $r\to\infty$, yet $\rho_1(r)$ approaches a constant for large r. The problem arises because we perform a full integration over the shadow variables in the shadow wave function.

A useful procedure is to sample the integrand of the single-particle density matrix:

$$\rho_1(r)=\mathcal{N}\int\int\int\int dR\,dS\,dS'\psi_r(\mathbf{r}_1+\mathbf{r},\mathbf{r}_2,\ldots,\mathbf{r}_N)\times\psi_r(\mathbf{r}_1,\mathbf{r}_2,\ldots,\mathbf{r}_N)\psi_s(S)\psi_s(S')\times\left[\theta(\mathbf{r}_1+\mathbf{r}-\mathbf{s}_1)\prod_{k=2}^{N}\theta(\mathbf{r}_k-\mathbf{s}_k)\right]\times\left[\prod_{l=1}^{N}\theta(\mathbf{r}_l-\mathbf{s}'_l)\right], \quad (19)$$

where $\mathcal{N}$ is an unknown normalization constant. $\rho_1(r)$ is then obtained by binning the value of r during the simulation. In other words, we perform a simulation where an extra particle is introduced. $N-1$ particles are still coupled to both sets of shadows, but now the Nth particle is coupled to only one of the sets and the $(N+1)$th to the other.

We combine Eq. (19) with the standard procedure which yields $\rho_1(r)$ accurately in the vicinity of $r=0$ to determine the normalization constant. Scaling $\rho_1(r)$ obtained from Eq. (19) to match the $\rho_1(r)$ of Eq. (16) computed at small values of r (typically $r<\sigma=2.556$ Å) results in a complete, normalized $\rho_1(r)$. Moreover since the statistical errors in the computation of $\rho_1(r)$ by Eq. (16) at small values of r are smaller than those obtained by Eq. (19), our final $\rho_1(r)$ is obtained through Eq. (16) for values of r less than ~ 1.3 Å and from Eq. (16) otherwise.

The fraction of particles in the zero momentum state, n_0, calculated at 0.0218 Å^{-3} using the $M+M(S)$, $M+A(S)$ and $O2B+A(S)$ wave functions is shown in Table IV. The GFMC n_0 of Panoff and Whitlock[31] is also given there, along with their variational result[31] using a wave function which contains both Jastrow correlations of the McMillan form and three-body correlations. When the $M+M(S)$ result of 4.51±0.03% was first obtained, its clear disagreement with GFMC condensate fraction was disappointing. As can be seen from the table, most of this discrepancy is overcome by the form for the shadow pseudopotential contained in the $M+A(S)$ form which yields 7.8±0.1% for n_0. The $O2B+A(S)$ shadow form yields 8.1±0.4. These results also represent a substantial improvement over the 5.62±0.05% variational result for the McMillan-Jastrow form with triplet correlations.[31] Also at the higher density 0.0262 Å^{-3} the $028+A(S)$ value of n_0 is in reasonable agreement with the GFMC value.

The condensate fractions obtained with the shadow wave functions are especially interesting in light of the following observation. Jastrow wave functions with McMillan correlations yield a condensate fraction of about 11%,[1] while Jastrow wave functions optimized using the paired-phonon analysis[32] (PPA) of Chang and Campbell yield a condensate fraction at the equilibrium density of 10.60±0.02%.[31] The incorporation of three-body correlations into the McMillan wave function depresses the condensate fraction to 5.62±0.05%,[31] far below the GFMC and experimental values. The shadow wave functions, which include correlations of all orders between the particles, show substantially improved condensate fractions compared with the McMillan form combined with explicit three-particle correlations. This is the first occasion when a variational wave function has yielded good results for both the energy of the fluid phase and the condensate fraction.

TABLE IV. The table shows results for the condensate fraction of our wave function at the equilibrium and freezing densities together with those from the literature. When reporting GFMC results, we give the importance function used in the calculation; J(PPA) denotes a functional optimization of the Jastrow factors by the paired-phonon analysis (Ref. 38).

ρ (Å^{-3})	Wave function	n_0 (%)
0.0218	$M+M(S)$ (Ref. 9)	4.51±0.03
	$M+A(S)$	7.8 ±0.1
	$O2B+A(S)$	8.1±0.4
	J(PPA) (Ref. 31)	10.69±0.02
	$M+T$ (Ref. 3)	5.62±0.05
	GFMC[J(PPA)] (Ref. 31)	9.35±0.05
	GFMC[$M+T$] (Ref. 31)	7.98±0.08
0.0262	$M+A(S)$	3.1±0.3
	GFMC[J(PPA)$+T$] (Ref. 23)	3.8±0.2

V. RESULTS FOR THE SOLID PHASE

The organization of our solid-phase results follows the patterns established in the liquid phase. We first compare our variational energies with the solid phase GFMC results of Whitlock and Panoff[23] for systems of 108 particles. Then our results are compared with those for the original shadow wave function having the repulsive McMillan form for the shadow pseudopotential. The use of the basis-set method in the solid phase is discussed, and comparisons are made with the variational results of Vitiello and Schmidt.[11] The equation of state for the solid phase is then presented together with the melting-freezing transition densities. We present the pair-correlation functions of the real and shadow systems. Finally, results for the single-particle distribution about a lattice site are presented and discussed.

The variational results that we report here are for simulations carried out on systems of 108 particles. Simulations were also carried out on systems of 256 particles, as a check on the stability of the crystal. We observed that there are regions of the $M+A(S)$ parameter space, characterized by large values of the parameter δ (≈ 0.24 compared with optimal values of ≈ 0.1), that describe a crystal phase that is unstable. Simulations on these unstable crystal systems with 256 particles show a rapid evolution ($\approx 10\,000$ Monte Carlo passes) from the initial fcc lattice to a state containing large regions with very few particles, or voids. This suggests that systems under these conditions have collapsed, with the voids an artifact of the fixed volume of the simulation cell and the strong attraction (large value of δ) between shadow particles. No indication of metastability is seen in the smaller (108 particles) system with the same parameter sets, even in very long runs. The stability of the crystalline state whose properties we describe below has been tested using long runs on systems of 108–500 particles, and no evidence of instability has been found.

In this work we explore the fcc solid, by our choice of the initial condition and by the shape of the simulation cell. An interesting question is the following: which is the lowest energy crystalline phase for the shadow wave function? It is known[33] from GFMC computations with the Lennard-Jones potential, that the energies of the fcc and of the hcp solids are very close. We might expect that a similar small difference is given by the shadow wave function so that to address the issue of the lowest energy crystalline phase would require a major numerical effort.

A. Energy

The variational, kinetic, and potential energies for the $M+A(S)$ and $O2B+A(S)$ form wave functions at three densities in the solid phase are shown in Table V. In the same table we show variational results from the literature for the $M+M(S)$ shadow function and for the $O2B+T+G$ function, a wave function with optimized two-body and triplet correlations together with one-body Gaussian localization factors.[11] We also show GFMC results. The solid phase was studied at the three densities $\rho=0.0294$, 0.0329, and 0.0353 Å^{-3}, where the first is the GFMC melting density.

1. *Comparison of $M+A(S)$ with GFMC*

At the two lowest densities in the solid phase, the $M+A(S)$ form yielded energies about 0.6 K above the GFMC energies. At the highest density this difference is 0.75 K. We computed the GFMC energy at our inter-

TABLE V. The table shows variational energies (E_T), together with the kinetic (E_K) and potential (E_V) energies for our $M+A(S)$ and $O2B+A(S)$ form wave functions. We also include the result for original, $M+M(S)$[9] form shadow wave function, and the $O2B+T+G^*$ variational result of Vitiello and Schmidt (Ref. 11). The GFMC result is that of Kalos *et al.* (Ref. 13).

ρ (Å^{-3})		E_T	E_K	E_V
0.0294				
	$M+A(S)$	−5.052±0.014	25.379±0.015	−30.431±0.019
	$O2B+A(S)$	−5.414±0.011	25.531±0.019	−30.945±0.014
	$M+M(S)_{n=5}$	−4.968±0.011	25.371±0.018	−30.339±0.020
	$O2B+T+G$[a]	−5.409±0.051	24.66±0.18	−30.07±0.16
	GFMC	−5.61±0.03	25.70±0.07	−31.31±0.07
0.0329				
	$M+A(S)$	−3.639±0.012	30.698±0.023	−34.337±0.031
	$O2B+A(S)$	−3.765±0.012	30.362±0.025	−34.127±0.024
	$M+M(S)_{n=12}$	−3.557±0.010	30.675±0.022	−34.232±0.010
	$O2B+T+G$	−4.011±0.036		
	GFMC[b]	−4.197±0.03		
0.0353				
	$M+A(S)$	−1.947±0.012	34.885±0.037	−36.831±0.035
	$O2B+A(S)$	−2.132±0.012	34.643±0.022	−36.775±0.017
	$O2B+T+G$	−2.368±0.042		
	GFMC	−2.70±0.06	33.3±0.2	−36.0±0.1

[a]The $O2B+T+G$ result quoted here is for a density of 0.0293 Å^{-3}.
[b]The GFMC result at 0.0329 Å^{-3} was interpolated from results at 0.0315 and 0.0335 Å^{-3}.

mediate density 0.0329 Å^{-3} by an interpolation of the results given in Ref. 23, while for the kinetic and potential energies no such interpolation has been carried out. At the GFMC melting density the variational kinetic energy is about 0.3 K lower than GFMC, while at the highest density 0.0353 Å^{-3} it is about 1.6 K larger than that result. At melting the variational potential energy is about 0.9 K above GFMC, while at the highest density the potential energy is 0.8 K lower. Overall, the solid phase variational energies share with those of the liquid phase the property that the difference between the variational energies and the GFMC eigenvalues are only a weak function of the density.

2. *Comparison of $M+A(S)$ with the $M+M(S)$ form shadow wave function*

The improvements in the variational energies of the solid phase of the $M+A(S)$ form compared with the $M+M(S)$ form are not as large as those seen in the liquid phase. At both the GFMC melting density and at 0.0329 Å^{-3}, the $M+A(S)$ energy is only about 0.08 K lower than the $M+M(S)$ energy. This compares with the typical 0.4–0.5 K energy reductions of the liquid phase. It is unlikely that the disparity in improvements seen in the two phases is due to an incomplete optimization of the parameters, as the variational search was very thorough. The large improvement over the early shadow wave function seen in our liquid phase variational energies has brought the description of the liquid phase into the same realm of agreement with GFMC as that of the solid phase.

3. *The basis-set method in the solid phase*

In order to study the solid phase using their basis-set optimization technique, it was necessary for Vitiello and Schmidt[11] to modify the form of their liquid phase wave function. This modification consisted of multiplying the original $O2B+T$ wave function by a product of Gaussian single-particle orbitals that localized the atoms in the vicinity of their lattice sites.

Because the shadow wave function yields a stable crystal phase without such explicit Gaussian localization factors, the same basis-set description of the real pseudopotential that was used in our liquid phase calculations can be carried over directly to the solid. We have included these results in Table V, and refer once again to that wave function as $O2B+A(S)$.

4. *Comparison of $M+A(S)$ with other variational results*

At the melting density the $O2B+T+G$ variational energy is lower by about 0.36 K than our $M+A(S)$. The comparison is nearly the same at the intermediate density 0.0329 Å^{-3}. At the highest density, 0.0353 Å^{-3}, the $O2B+T+G$ form yields an energy 0.42 K lower than $M+A(S)$. This trend as a function of density differs from that seen in the liquid phase, where as the density increased the difference between our energy and that of the $O2B+T+G$ form increased substantially.

At melting the $O2B+A(S)$ shadow form yields a variational energy equivalent to that of $O2B+T+G$. As the density increases above melting, $O2B+A(S)$ yields a variational energy about 0.24 K above that of $O2B+T+G$.

TABLE VI. Fitting coefficients in the equation of state curve in the solid phase for the $M+A(S)$ and $O2B+A(S)$ variational results. The GFMC result of Kalos *et al.* (Ref. 13) is also shown. We have elected to make our fit to a polynomial of the form $E/N=A+B[(\rho-\rho_1/\rho_1)]^2+C[(\rho-\rho_1/\rho_1)]^3$, where $\rho_1=0.4486$ is taken from the GFMC result.

	$M+A(S)$	$O2B+A(S)$	GFMC
A	−5.34±0.021	−5.81±0.02	−5.899±0.023
B	31.00±1.50	47.7±1.4	31.95±5.26
C	9.92±4.34	−33.89±4.14	3.395±80.0

5. *Equation of state*

Because our parameter optimization has been carried out at only three densities in the solid phase, the four parameter polynomial fit to the energies that was carried out in the liquid phase cannot be directly carried over to the solid phase. Instead we have elected to make our fit to a polynomial of the form

$$\frac{E}{N}=A+B\left[\frac{\rho-\rho_1}{\rho_1}\right]^2+C\left[\frac{\rho-\rho_1}{\rho_1}\right]^3,$$

where the value of ρ_1 is taken to be the same as the GFMC result of Kalos *et al.*,[13] $\rho_1=0.026\,86$ Å. With this parameter fixed, the results of fitting this polynomial to our solid phase energies are shown in Table VI along with the GFMC values. Our $M+A(S)$ form shows good agreement with GFMC with the exception of a discrepancy in the constant term A. In other words our variational energies are uniformly higher than the exact energies.

B. The optimum variational parameters

Table VII shows the optimum variational parameters of the $M+A(S)$ form wave function. A fundamental feature of the shadow form wave functions is that they provide good descriptions of both the solid and liquid phases. The form is the same in both phases so that only the parameters change with density.

Comparisons of Tables III and VII show that there is a decrease in the power law b of the real particle pseudopotential in moving from the liquid to the solid phase. The parameter α, which does not vary strongly with density in the liquid phase, shows a much greater variation in the

TABLE VII. The optimum variational parameters of the $M+A(S)$ form wave function in the solid phase are tabulated.

ρ (Å^{-3})	b (Å)	C (Å^{-2})	δ (K^{-1})	α
0.0294	2.760	0.8725	0.11	0.875
0.0329	2.799	0.9031	0.10	0.890
0.0353	2.799	0.9949	0.11	0.900

solid phase, increasing with density. Similarly, the real-shadow interaction strength C increases more rapidly with density in the solid phase than in the liquid phase.

Comparing the shadow-shadow pair-correlation function at melting with that of a set of classical particles whose distribution function was taken as $|\psi_s(S)|^2$ (i.e., which interacted through an Aziz-form potential at an effective temperature), we discovered that these functions were quite similar. The corresponding comparison between the pair-correlation function for the real particles and that of the classical system distributed according to $|\psi_r(R)|^2$ showed that in contrast, these functions differed remarkably. These results were in accordance with our original intuition that it is primarily the shadow-shadow pseudopotential, rather than that of the real particles, that determines the structure of the real particle system.

Later in the paper we will give a detailed discussion of the Lindemann ratio for solid helium described by the shadow wave function. From that discussion we will conclude that the "melting" of the shadow particles shows considerable similarity with the melting of a classical system.

A comparison of the values of our C with the parameters that describe the Gaussian localization strengths of other wave functions suggests that in each, these parameters play a quantitatively different role. Vitiello *et al.*[9] found that for a Nosanow-Jastrow form, Eq. (17) wave function at $\rho=0.329$ Å^{-3}, the optimum Gaussian localization parameter is 0.735 Å^{-2}. The value of the Gaussian localization strength from the optimization of the $O2B+T+G$ wave function[11] at the same density is 0.6122 Å^{-2}. Our value of our Gaussian parameter C, is $=0.9031$ Å^{-2}, considerably larger than either of these others. The same comparison with the $O2B+T+G$ results at the remaining two densities in the solid phase leads to a similar conclusion: the real particles in the solid phase of the shadow wave function are localized to a much greater extent near their shadow particles than the ^{4}He atoms of other variational studies are near their lattice sites. This observation is not surprising, as the delocalization of atoms in the solid phase of the shadow wave function arises from both the distribution of the real particles about their shadow partners and from the distribution of the shadow particles about their lattice sites.

C. The radial distribution function

The spherically averaged radial distribution functions for the $M+A(S)$, $O2B+A(S)$, and $M+M(S)$ forms are shown at melting in Fig. 7(a). Figure 7(a) also shows the GFMC result at melting. The pair-correlation functions of both our shadow wave functions are nearly in agreement with one another and with the GFMC $g(r)$ at melting. The two are also in agreement at 0.0329 Å^{-3}.

Figure 7(b) shows the shadow-shadow correlation function $g(s)$ at the melting density. A trend in the liquid phase also present in the solid is that the $g(s)$ for our form shows greater shadow correlations, and especially an enhanced nearest-neighbor peak, than the $M+M(S)$ form.

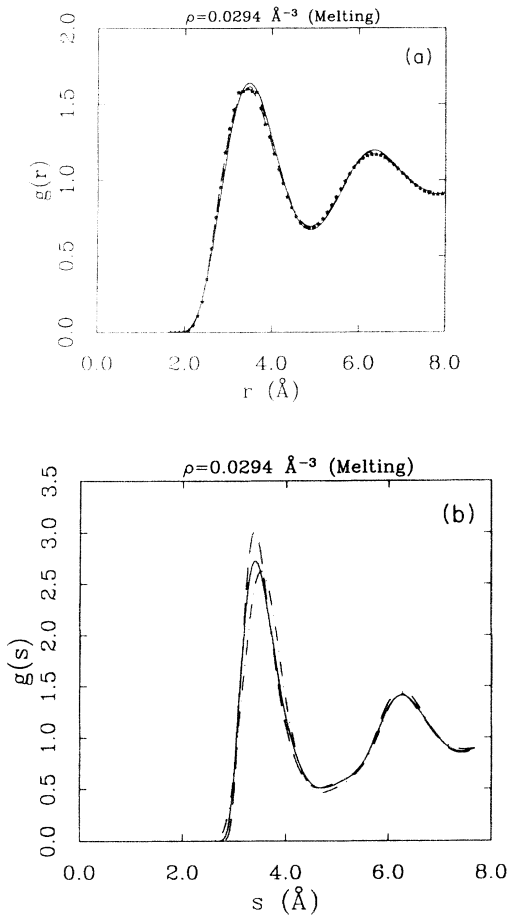

FIG. 7. (a) and (b) The figures show the pair-correlation functions of both the real and shadow systems at the melting density. The smooth curve is $M+A(S)$, dashes denote $O2B+A(S)$ and dash-dot denotes $M+M(S)$. Stars in (a) denote GFMC results.

D. The single-particle distribution function

1. *The Lindemann ratios*

The Lindemann ratio γ_L of a solid is defined as the ratio at melting of the square root of the second moment of the singlet distribution function of an atom about its lattice site to the nearest-neighbor distance of a perfect lattice. Simulations on classical[34] and quantum[35] systems confirm the theoretical expectation that the Lindemann ratio is strongly dependent on the size of the system considered. This size dependence comes about because the mean square of the displacements from the lattice sites is dominated by long-wavelength phonon modes.

There is an important quantitative difference in the size dependences of the second moment of the lattice site distributions of classical and quantum systems. Noting that microscopic structure is unimportant in determining the long-wavelength vibrational modes, Young and Alder[34] argued that the Debye model yields the correct functional dependence of the lattice site distribution on size. This gives for the dependence of the Lindemann ratio γ_L on

system size

$$\gamma_{L,N}=\gamma_{L,\infty}\sqrt{1+KN^{-1/3}}\ , \tag{20}$$

where $\gamma_{L,N}$ is the Lindemann ratio for a system of N particles and $\gamma_{L,\infty}$ is that result in the thermodynamic limit. K is a parameter independent of N, typically of order unity. This scaling form (and the analogous one in two dimensions) was found by Young and Alder to describe well the size dependence of classical systems of hard disks and spheres. The quantum-mechanical argument follows a similar line of reasoning, with the result that in addition to a finite temperature phonon contribution a size dependence from zero-point motion of phonons is present in the ground state. In the quantum ground state, with no phonon modes excited, the only size dependence arises from the zero-point phonon motion. One finds that

$$\gamma_{L,N}=\gamma_{L,\infty}\sqrt{1+K'N^{-2/3}}\ , \tag{21}$$

where K' is a constant. For typical systems of 10^2–10^3 particles, the finite-size corrections suggested by these expressions, especially Eq. (20), can be substantial.

The two forms given above, classical and quantum, raise the question of which if either describes the scaling of the shadow wave function. The exact ground-state wave function should have the scaling form (21), as a result of the infinite range correlations induced by zero-point phonons. Reatto and Chester[17] showed that if the infinite range correlations induced by phonons are to be correctly incorporated into a wave function, the pseudopotential must asymptotically have the form $\chi(r)\propto r^{-2}$. Correlations of this form are a necessary ingredient in the proper linear behavior of the structure factor for small wave vectors, as well as in the correct asymptotic form for $g(r)$. The pseudopotential used in the present study does not have this asymptotic long-range behavior and we are led to expect, on this basis, that the classical scaling (20) form should be appropriate for the shadow wave function.

Table VIII (top) shows the Lindemann ratios for our $M+A(S)$ wave function together with those of the $M+M(S)$ form for systems of 108, 256, and 500 particles. Results are shown for both the real and shadow systems. We carried out fits to these results, testing both (20) and (21). As we expect, the Lindemann ratios were found to scale according to Eq. (20). Table VIII (bottom) shows the values of the constant K in the fit, together with the extrapolated infinite system Lindemann ratios $\gamma_{L,\infty}$ of both the real and shadow systems.

Table VIII (bottom) illustrates the dependences of the Lindemann ratios of both the real and shadow systems on the system size. The constant K of Eq. (20) shows that the shadow particles have the strongest size dependence, both for the $M+A(S)$ and for the original $M+M(S)$ wave functions. Both systems of the $M+M(S)$ form have greater size dependences than those of the $M+A(S)$ form. It is interesting that while the real particle extrapolated Lindemann ratios of $M+M(S)$ system are substantially larger than those of the $M+A(S)$ form, the extrapolated ratios for the shadow particles differ only slightly.

The melting of classical crystalline systems is known to conform to a remarkable degree to the empirical Lindemann melting law, which states that such systems will melt when the Lindemann ratio reaches a critical value which depends only weakly on the interaction potential. Simulations on systems interacting through power-law potentials[36] show the critical Lindemann ratios range from around 0.13 for hard spheres (the infinite power case) to 0.18 for the soft $n=4$ power. Lennard-Jones systems melt when this ratio is about 0.145. The melting of quantum systems does not conform to this simple criterion. Although the Lindemann ratio of the real particles is much larger than the classical critical value for any potential simulated, an analogy between shadows and a system of classical particles arising from the high degree of structure seen in their pair correlations suggests that we explore the applicability of the Lindemann melting law to the shadows. As shown in Table VIII (bottom), while the extrapolated shadow Lindemann ratios are considerably smaller than those of the real particles, they are still larger than any seen classically. We note, however

TABLE VIII. (Top) Our Lindemann ratios for the $M+A(S)$ form wave function are shown in the table, together with the $M+M(S)$ result of Vitiello *et al.* (Ref. 9). These results are shown for both the real and shadow particles. Results are shown for systems of 108, 256, and 500 particles. (Bottom) Extrapolated infinite system Lindemann ratios and scaling constants K. The results for both the real and shadow systems are shown in each case.

N	Wave function	Real Lindemann ratio	Shadow Lindemann ratio
108	$M+M(S)$	0.2488	0.1763
	$M+A(S)$	0.2402(2)	0.1816(2)
256	$M+M(S)$	0.2545	0.1842
	$M+A(S)$	0.2449(3)	0.1880(2)
500	$M+M(S)$	0.2576	0.1886
	$M+A(S)$	0.2478 (1)	0.1924 (1)

Wave function	Real $\gamma_{L,\infty}$	Real K	Shadow $\gamma_{L,\infty}$	Shadow K
$M+M(S)$	0.2703	−0.7280	0.2054	−1.25
$M+A(S)$	0.2587	−0.6585	0.2073	−1.112

that in the square of the wave function two shadows are attached to each particle, so that a more appropriate comparison is based on the mean position of the two shadows. Since there is no interaction between the two shadows of one particle we can take as a first approximation that there is no correlation between the displacements of the two shadows from their common equilibrium position. In this case the Lindemann ratio for the mean position of the shadows is $1/\sqrt{2}$ times the shadow γ_L, i.e., about 0.15. Correlations between displacements of the shadows will increase this value a bit, but it should remain in the range appropriate for classical monatomic particles with soft repulsive forces. This conclusion supports our contention that the shadow variables behave in a rather classical fashion.

2. *The moments of the singlet distribution function*

A further widely used probe of the one-body distribution of atoms about their lattice site is the ratio of moments of this distribution. In particular we consider ratios of two such moments that for a perfect Gaussian distribution are unity. The ratios that we have computed are $\langle r^6\rangle/\frac{35}{9}\langle r^2\rangle^3$ and $\langle r^4\rangle/\frac{5}{3}\langle r^2\rangle^2$. Simulations on classical hard-sphere systems have shown that the singlet distributions have small deviations from the Gaussian form over a range of densities.[34] Such non-Gaussian distributions have been observed in quantum simulations of ^{4}He,[37] but to a much lesser extent than is seen classically near melting. The values of the ratios that we give here characterize the singlet distribution function in the following way: ratios which are larger than 1 reveal a lattice site distribution which is broader than a perfect Gaussian, while values less than unity show a distribution more narrow than Gaussian.

The second, fourth, and sixth moments of the lattice site distribution at 0.0329 Å^{-3} for 108 particles are shown in Table IX. Table X shows the ratios of these moments which should be unity for a perfect Gaussian distribution. The moments of our distribution and that of $M+M(S)$ wave function are in agreement. The ratios of moments in Table X show that at this density, for both trial wave functions, the one-body lattice-site distributions are slightly broader than Gaussian. Our wave function also shows a slightly broader distribution than was seen with the $M+M(S)$ form.

VI. THE MELTING-FREEZING TRANSITION

Using our two polynomial expressions for the energy in the solid and liquid phases for the $M+A(S)$ wave function, we have carried out the usual Maxwell double-tangent construction to determine the freezing and melting densities ρ_f and ρ_m. We find that $\rho_f=0.025\,69\pm0.0006$ Å^{-3} and $\rho_m=0.0294\pm0.0004$ Å^{-3}, in excellent agreement with the GFMC transition densities, $\rho_f=0.0262\pm0.0007$ Å^{-3} and $\rho_m=0.0294\pm0.0006$ Å^{-3}. These good melting-freezing densities are further encouragement that shadow wave functions may provide a good tool for studying this phase transition in ^{4}He systems.

TABLE IX. The table shows the moments of the singlet distribution about a lattice site at $\rho=0.0329$ Å^{-3} in the solid phase. We show our $M+A(S)$ results together with those of the $M+M(S)$ form. These results are from simulations on 108 particle systems.

	$\langle r^2\rangle$	$\langle r^4\rangle$	$\langle r^6\rangle$
$M+M(S)$	0.651±0.05	0.717±0.042	1.115±0.084
$M+A(S)$	0.629±0.001	0.671±0.003	1.018±0.006

TABLE X. The table shows ratios of moments of the single-particle distribution about a lattice site for the $M+M(S)$ and our $M+A(S)$ form at $\rho=0.0329$ Å^{-3}.

	$\langle r^4\rangle/\frac{5}{3}\langle r^2\rangle^2$	$\langle r^6\rangle/\frac{105}{27}\langle r^2\rangle^3$
$M+M(S)$	1.014±0.0017	1.042±0.005
$M+A(S)$	1.0172±0.008	1.052±0.004

VII. DISCUSSION

Our exploration of the scaled-Aziz form for the shadow pseudopotential represents a thorough study of the shadow wave function. This form provides a good description of solid and liquid ^{4}He, and in particular brings the description of the liquid phase to the same level of agreement with GFMC that was achieved previously in the solid phase. Because the optimization of the parameters of the original $M+M(S)$ shadow wave function was carried out at only a small number of densities in the liquid phase, the extraction of an equation of state from those results was not possible. The great discrepancy in the agreement of the liquid and solid phase variational energies with GFMC strongly suggests, however, that a very poor equation of state would have resulted. We now have a substantial reduction in variational energies at all densities in the liquid phase. This improvement over the original shadow wave function leads to an equation of state that is in good agreement with the GFMC result. In particular our melting and freezing densities agree closely with those derived from GFMC.

In addition to the improved variational energies, the $M+A(S)$ form also shows improved structural properties in the liquid phase compared with the early shadow wave function. In particular the pair correlations show a substantial improvement compared with those obtained from the original shadow wave function. The condensate fraction obtained from our form makes up the greatest part of the difference between that of the early shadow function and GFMC. We regard this as one of our most significant results.

A further improvement of the shadow wave function is obtained if the McMillan form of the pseudopotential for the real particles is replaced by a basis-set optimized form. The lowering of variational energy is especially great at the melting and freezing densities, yielding the lowest variational energies obtained with variational

Monte Carlo. The reduction in energy is not as great at the equilibrium density and as a consequence the equation of state has an anomalous behavior.

This work demonstrates the usefulness of including high-order particle correlations into a wave function via the introduction of subsidiary variables rather than through the explicit introduction of a high-order particle pseudopotential into a trial wave function. While the shadow wave function possesses a complex many-body pseudopotential (albeit hidden in the integration over shadow particles), the shadow particles provide a simple, intuitive interpretation of that pseudopotential.

ACKNOWLEDGMENTS

We would like to acknowledge a number of useful discussions with Shiwei Zhang. This work is supported by the Condensed Matter Theory Program of the National Science Foundation under Grant No. DMR-9200469 and by Consorzio INFM. Tom MacFarland is financially supported by the Department of Education under Grant No. P200A10148-93. A part of this work was carried out using resources of the Cornell Theory Center, which is funded by the US National Science Foundation, by New York State, by IBM, and by Cornell University.

[1]W. L. McMillan, Phys. Rev. **138**, A442 (1965).
[2]S. A. Vitiello, K. Runge, and M. H. Kalos, Phys. Rev. Lett. **60**, 1970 (1988).
[3]W. Wu, S. A. Vitiello, L. Reatto, and M. H. Kalos, Phys. Rev. Lett. **67**, 1446 (1991).
[4]S. A. Vitiello, L. Reatto, M. H. Kalos, and G. V. Chester, Physica B **194/196**, 699 (1994).
[5]F. Pederiva, A. Ferrante, S. Fantoni, and L. Reatto, Phys. Rev. Lett. **72**, 2589 (1994).
[6]S. Zhang, M. H. Kalos, G. V. Chester, S. A. Vitiello, and L. Reatto, Physica B **194-196**, 523 (1994).
[7]L. H. Nosanow, Phys. Rev. **146**, 120 (1966).
[8]D. N. Levy and C. W. Woo, Phys. Rev. B **13**, 3750 (1976).
[9]S. A. Vitiello, K. J. Runge, G. V. Chester, and M. H. Kalos, Phys. Rev. B **42**, 228 (1990).
[10]L. Reatto and G. L. Masserini, Phys. Rev. B **38**, 4516 (1988).
[11]S. A. Vitiello and K. E. Schmidt, Phys. Rev. B **46**, 5442 (1992).
[12]R. A. Aziz, V. P. S. Nain, J. S. Carley, W. L. Taylor, and G. T. McConville, J. Chem. Phys. **70**, 4330 (1979).
[13]M. H. Kalos, M. A. Lee, P. A. Whitlock, and G. V. Chester, Phys. Rev. B **24**, 115 (1981).
[14]D. Chandler and P. Wolynes, J. Chem. Phys. **74**, 4078 (1981).
[15]R. P. Feynman and A. R. Hibbs, *Quantum Mechanics and Path Integrals* (McGraw-Hill, New York, 1965).
[16]Because we use periodic boundary conditions we must make $u(r)$ and its first two derivatives vanish at the side of the simulation cell. For this reason, at some distance r_m close to the side of the cell, $u(r)$ takes the form $u(r) = \text{constant} \times (r - r_m)^3$. In order that $u(r)$ be continuous at r_m, a constant offset is added to $(b/r)^5$.
[17]L. Reatto and G. V. Chester, Phys. Rev. **155**, 88 (1967).
[18]Jack Zwanziger, Ph.D. thesis, Cornell University, 1972.
[19]V. R. Pandharipande and H. A. Bethe, Phys. Rev. C **7**, 1312 (1973).
[20]O. Penrose and L. Onsager, Phys. Rev. **104**, 576 (1956).
[21]We have recently observed that when a helium system of 108 particles is started from a completely random initial configuration it will spontaneously crystallize during a long Monte Carlo run. The system is treated variationally using the shadow wave function of this paper. We found that crystallization into a face-centered-cubic lattice occurred during runs of between 10^5 and 10^6 Monte Carlo sweeps. The same phenomenon has been observed by Reatto using a shadow wave function in which the variational parameters depend on the *local* density in the system.
[22]D. M. Ceperley and M. H. Kalos, *Quantum Many-Body Problems,* Monte Carlo Methods in Statistical Physics, 2nd ed., edited by K. Binder (Springer-Verlag, Berlin, 1986).
[23]P. Whitlock and R. M. Panoff, Can. J. Phys. **65**, 1409 (1987).
[24]Pat T. Roach, J. B. Ketterson, and Chia Wei Woo, Phys. Rev. A **2**, 543 (1970).
[25]K. Schmidt, M. H. Kalos, and Michael A. Lee, Phys. Rev. Lett. **45**, 7 (1980).
[26]D. M. Ceperley and G. V. Chester, Phys. Rev. A **15**, 755 (1977).
[27]It was observed that the $S(\mathbf{k})$ calculated from Eq. (14) showed a high degree of anisotropy for small $\mathbf{k}$ in the 32 particle simulations that persisted into the region of the large peak in $S(k)$. These were greatly diminished in the 108 particle simulation, and in the 256 particle simulation were only seen for $|\mathbf{k}| < 1.5$ Å.
[28]E. C. Svensson, V. F. Sears, A. D. B. Woods, and P. Martel, Phys. Rev. B **21**, 3638 (1980).
[29]V. F. Sears, E. C. Svensson, A. D. B. Woods, and P. Martel (unpublished).
[30]F. H. Wirth and R. B. Hallock, Phys. Rev. B **35**, 89 (1987).
[31]R. M. Panoff and P. A. Whitlock, in *Momentum Distributions in Quantum Liquids from Green's function Monte Carlo Calculations,* Proceedings of the Workshop on Momentum Distributions, Argonne, Illinois, October, 1988, edited by R. N. Silver and P. E. Sokol (Plenum, New York, 1989).
[32]C. C. Chang and C. E. Campbell, Phys. Rev. B **15**, 4238 (1977).
[33]P. A. Whitlock, M. H. Kalos, G. V. Chester, and D. M. Ceperley, Phys. Rev. B **21**, 999 (1980).
[34]David A. Young and Berni J. Alder, J. Chem. Phys. **60**, 1254 (1974).
[35]Pak-wo Leung, Ph.D. thesis, Cornell University, 1990.
[36]Ronald D. Peterson, Ph.D. thesis, Cornell University, 1980.
[37]P. A. Whitlock, D. M. Ceperley, G. V. Chester, and M. H. Kalos, Phys. Rev. B **19**, 5598 (1979).
[38]F. J. Pinski and C. E. Campbell, Phys. Lett. **79B**, 23 (1978).

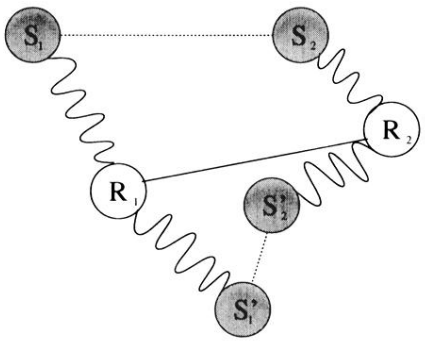

FIG. 1. The figure shows two of the classical trimers which arise when the Metropolis algorithm is used to sample the modulus squared of the shadow wave function. The continuous line represents the real particle pseudopotential $u(r)$ and the dotted lines that of the shadows, $w(s)$. The labels on each monomer designate the system to which that monomer belongs, either the real or one of the two shadow sets.